ELECTRONIC SUPPLEMENTARY INFORMATION

"Amidoboranes of rubidium and caesium: the last missing members of the alkali metal amidoborane family"

Rafał Owarzany[1,2], Tomasz Jaroń[1], Piotr J. Leszczyński[1], Karol J. Fijalkowski[1*], Wojciech Grochala[1]

1. Centre of New Technologies, University of Warsaw, ul. Banacha 2c, 02-097 Warsaw, POLAND
2. Department of Chemistry, University of Warsaw, ul. Pasteura 1, 02-089 Warsaw, POLAND

Contents:

1. Synthesis of alkali amidoboranes

We used the highest purity available precursors: metallic Rb (99,6%, Sigma Aldrich), metallic Cs (99,5%, Sigma Aldrich), LiH, NaH, $LiNH_2$, KH (all 95%, Sigma Aldrich) and NH_3BH_3 (97%, JSC Aviabor).

We synthesized RbAB and CsAB at room temperature using dry THF as a solvent, under argon atmosphere with no contact with atmospheric air, according to the following reaction equations:

$$Rb + NH_3BH_3 \rightarrow RbNH_2BH_3 + \tfrac{1}{2} H_2\uparrow$$
$$Cs + NH_3BH_3 \rightarrow CsNH_2BH_3 + \tfrac{1}{2} H_2\uparrow$$

Products are insoluble in THF. Solvent was decanted after sedimentation. Solid products were either left at room temperature until dry or vacuum dried. In case of CsAB vacuum drying was a necessity.

LiAB, NaAB and KAB were synthesized in a procedure described in our previous papers.

We synthesized LiAB and NaAB via a dry mechanochemical way using steel disk milling vessel of our construction together with a high energy mill from Testchem. All operations were carried out under argon atmosphere with no contact with atmospheric air, according to the reaction equations:

$$LiNH_2 + NH_3BH_3 \rightarrow LiNH_2BH_3 + NH_3\uparrow \qquad \text{2 times per 3 minutes of milling}$$
$$NaH + NH_3BH_3 \rightarrow NaNH_2BH_3 + H_2\uparrow \qquad \text{single 3 minutes milling}$$

We synthesized NaAB and KAB using dry THF as a solvent under argon atmosphere with no contact with atmospheric air, according to the following reaction equations. After the reaction, the solvent was desorbed at room atmosphere. Obtained products were of no need for other further processing.

$$NaH + NH_3BH_3 \rightarrow NaNH_2BH_3 + H_2\uparrow$$
$$KH + NH_3BH_3 \rightarrow KNH_2BH_3 + H_2\uparrow$$

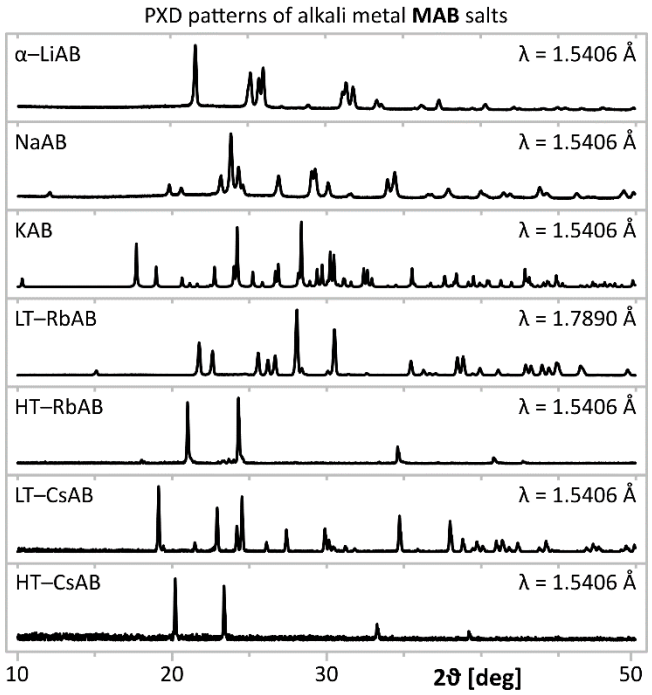

Fig. S1.1. Comparison of PXD patterns of alkali metal amidoboranes.

2. Spectra and table of 11B NMR @ THF-d8 chemical shifts of alkali metal amidoboranes

Table S2.1. Chemical shifts, position of multiplets and J-coupling values observed in ^{11}B NMR spectra in deuterated THF solutions (δ [ppm]) of alkali metal amidoboranes [LiAB, NaAB, KAB, RbAB, CsAB] at room temperature. Chemical shifts of fresh ammonia borane (AB) at room temperature are shown for comparison.

multiplet		amidoboranes				
	AB	LiAB	NaAB	KAB	RbAB	CsAB
BH_3 quartet	–18.184 –19.632 –21.144 –22.610	–18.100 –19.337 –20.120 –22.120	–19.900 –21.265 –22.568 –23.907	–19.976 –21.469 –22.948 –24.421	–20.524 –21.522 –22.533 –23.455	–20.708 –21.631 –22.699 –23.634
position	–20.393	–19.920 Hz	–21.910 Hz	–22.204 Hz	–22.009 Hz	–22.168 Hz
^1J (B,H)	95 Hz	86 Hz	86 Hz	95 Hz	94 Hz	94 Hz

^{11}B NMR spectra of LT-RbAB and LT-CsAB contain a quartet (1:3:3:1) at –22.1 ppm and –22.2 ppm respectively representing [BH_3] groups in amidoborate anions (Figure S2.2.). This is consistent with ^{11}B NMR spectra of light alkali metal amidoboranes showing similarity of $NH_2BH_3^-$ anions present in the crystal structures of the compounds. Smaller signal-to-noise ratio in the spectra of LT-RbAB and LT-CsAB in comparison with lighter amidoboranes is caused by their poorer solubility in THF. Spectra of LiAB, NaAB and KAB were collected using 200 MHz NMR spectrometer, while RbAB and CsAB using 300 MHz NMR spectrometer.

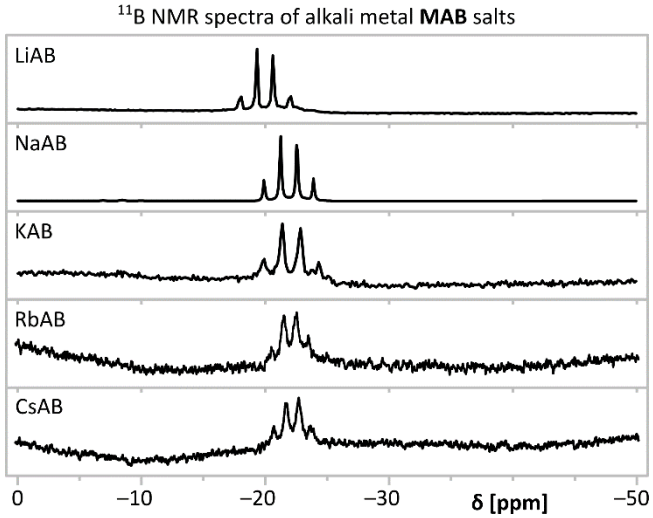

Fig. S2.2. Comparison ^{11}B NMR spectra of alkali metal amidoboranes.

3. Table of appearing bands in infrared absorption spectra of alkali metal amidoboranes

Table S3.1. Absorption bands detected in infrared absorption spectra (wavenumber [cm^{-1}]) of alkali metal amidoboranes [LiAB, NaAB, KAB, RbAB, CsAB] at room temperature. Absorption bands of fresh ammonia borane (AB) at RT are shown for comparison. (ν = stretching, δ = deformation: bending and torsional modes).

Band		amidoboranes				
	AB	LiAB	NaAB	KAB	RbAB	CsAB
ν(NH)			3393 vw			
			3380 vw			
		3370 sh	3369 vw			
		3359 m		3347 w		
			3329 vw		3344 vw	3347 w
	3311 vs	3310 w	3303 m	3300 vw	3303 vw	
		3273 vw				
	3253 vs	3251 vw	3256 w			3250 w
			3200 vw			
	3196 s	3185 sh				
ν(BH)						
	2347 vs	2326 m	2340 s	2331 w		2331 w
	2289 s	2280 sh	2289 s			
		2245 s	2224 s			
		2194 vs		2184 vs	2183 vs	2185 vs
		2152 s		2169 vs		2169 vs
	2118 m		2120 sh	2122 s	2119 vs	2122 s
		2035 sh	2065 sh	2082 s		2082 s
						2009 sh
δ(NH)	1611 m	1605 sh	1608 w	1608 vw	1601 w	1608 vw
		1570 w		1447 vw		1447 w
		1544 m	1532 s	1380 vw	1397 vw	1380 w
		1495 sh				
δ(BH)		1315 sh	1317 m		1231 s	1243 m
		1261 s	1260 sh	1243 m	1208 vs	1224 s
			1232 m	1224 s		1202 vs
			1198 vs	1202 vs	1162 m	
		1180 vs	1173 s		1129 w	1128 w
	1163 vs	1165 sh				
		1135 m	1129 w	1128 w		1061 vw
	1067 s	1065 sh	1074 w			
		1016m	999 w	1004 m	996 m	1004 m
ν(BN)		920 vw	922 vw		894 vw	887 w
		902 w	901 w		878 w	830 w
and			880 vw	887 w	831 w	789 w
other		842 w	837 w	830 w		
		800 m	797 w	789 w	738 m	752 w
		784 m	742 w	752 w		

4. Table of bands appearing in the Raman spectra of alkali metal amidoboranes

Table S4.1. Absorption bands detected in Raman scattering spectra (wavenumber [cm^{-1}]) of alkali metal amidoboranes [LiAB, NaAB, KAB, RbAB, CsAB] at room temperature. Absorption bands of fresh ammonia borane (AB) at RT are shown for comparison. (ν = stretching, δ = deformation: bending and torsional modes).

Band		amidoboranes				
	AB	LiAB	NaAB	KAB	RbAB	CsAB
ν(NH)		3361 s	3372 m	3347 w	3347 m	3333 s
	3314 m	3303 vs	3314 s			
				3297 w	3290 vs	
	3253 vs		3258 w			3248 w
	3177 m					
ν(BH)						
	2378 vs	2368 w	2376 w	2359 vw		2395 vw
		2327 sh			2327 w	2320 vw
		2317 sh	2307 vw			2273 vw
	2284 vs					
		2191 vs	2183 s	2183 vs	2197 vs	
		2153 s				2163 vs
			2103 m	2117 w	2127 w	2133 s
			2069 m	2078 w		2069 w
			1987 sh	2010 sh		2011 vw
δ(NH)		1650 vw	1646 vw			
	1598 m	1613 vw	1620vw	1630 vw	1597 vw	
	1583 m		1563 vw			
		1524 wv				
δ(BH)			1260 w			
			1242 w	1240 w	1229 vw	
			1202 vw		1205 vw	
	1190 sh			1197 w		1191 s
	1168 m	1152 m	1172 vw	1190 w	1164 w	1159 m
		1122 vw	1130 vw	1179 w		
	1069 vw					
		1021 vw	1001 vw	1005 vw		
ν(BN) and other		919 m	922 w	913 sh		998 vw
		901 s	904 m	903 sh		909 vw
				885 w	892 vw	893 w
					875 m	
	800 w	818 m	829 vw	822 vw	827 vw	826 vw
	785 m		764 w	777 vw		778 vw
	729w			746 vw	746 vw	
		603 w				
		584 w	594 vw			

5. Comparison of infrared absorption and Raman scattering spectra of alkali metal amidoboranes

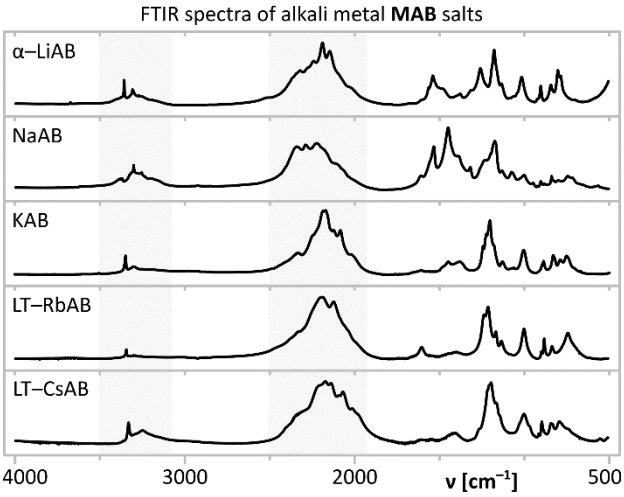

Fig. S5.1. Comparison of FTIR spectra of alkali metal amidoborane salts.

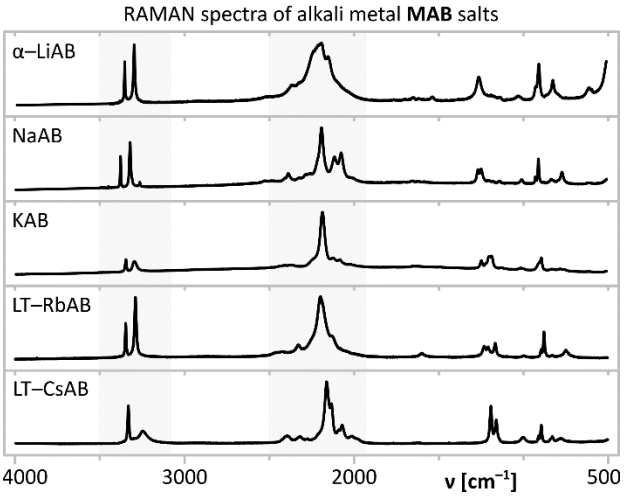

Fig. S5.2. Comparison of Raman spectra of alkali metal amidoborane salts.

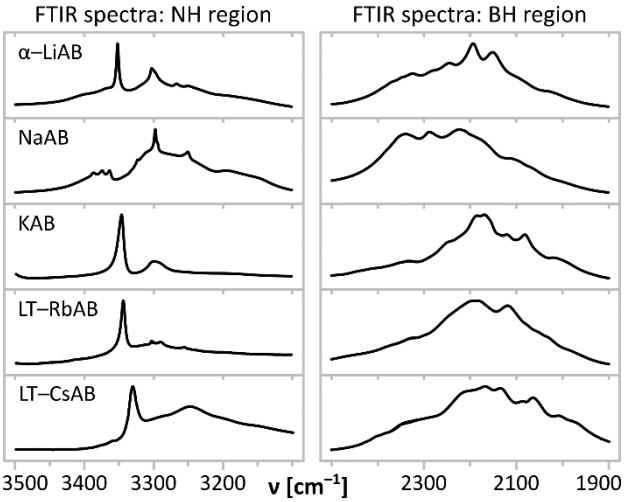

Fig. S5.3. Comparison of magnified NH stretching region and BH stretchinig region of FTIR spectra of alkali metal amidoborane salts.

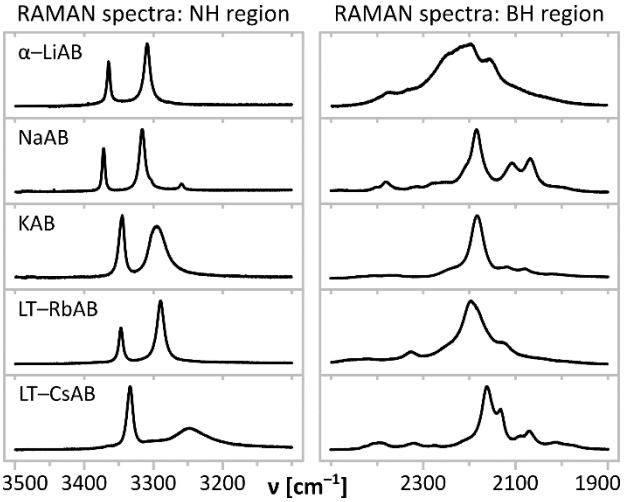

Fig. S5.4. Comparison of magnified NH stretching region and BH stretchinig region of RAMAN spectra of alkali metal amidoboranes salts.

.

6. Thermal decomposition (TGA/DSC/MS) of alkali metal amidoboranes

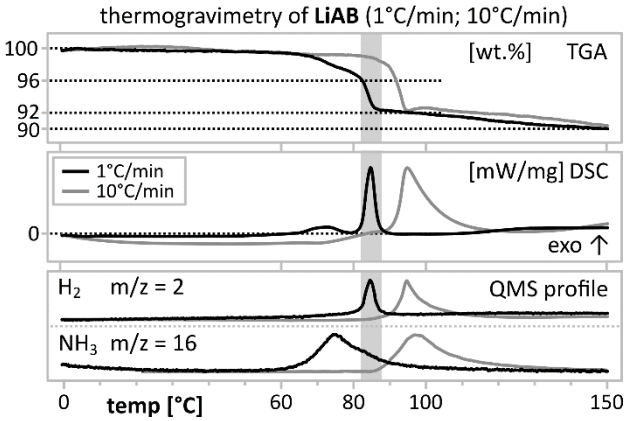

Fig. S6.1. TGA/DSC experiments of LiAB with two different scanning rates: 1°C/min and 10°C/min.

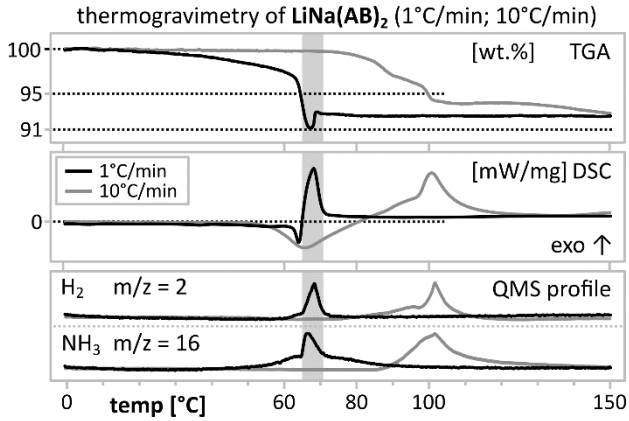

Fig. S6.2. TGA/DSC experiments of LiNa(AB with two different scanning rates: 1°C/min and 10°C/min.

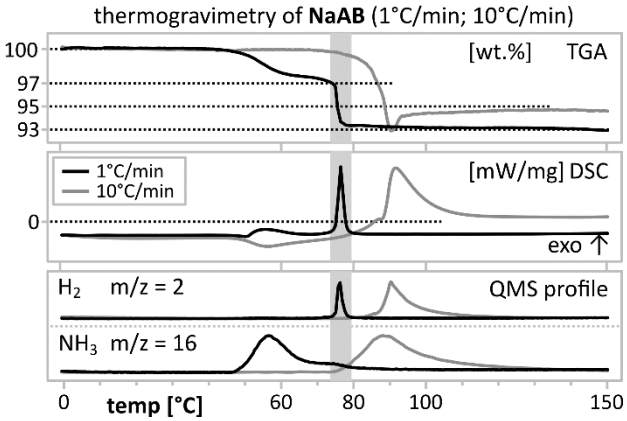

Fig. S6.3. TGA/DSC experiments of NaLi(AB)$_2$ with two different scanning rates: 1°C/min and 10°C/min.

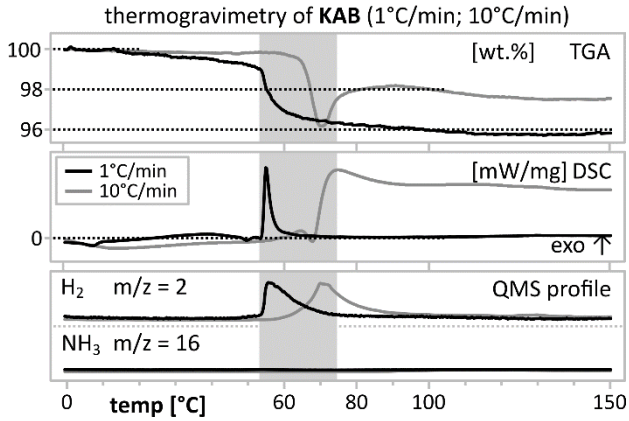

Fig. S6.4. TGA/DSC experiments of KAB with two different scanning rates: 1°C/min and 10°C/min.

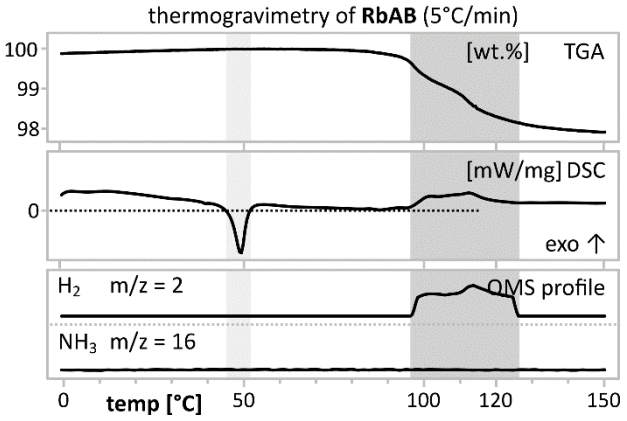

Fig. S6.5. TGA/DSC experiments of RbAB with a scanning rate: 5°C/min.

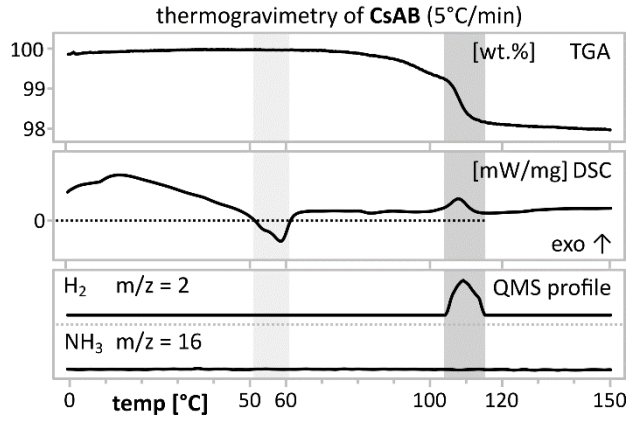

Fig. S6.6. TGA/DSC experiments of CsAB with a scanning rate: 5°C/min.

7. Decomposition of rubidium and caesium amidoboranes upon thermal treatment and aging

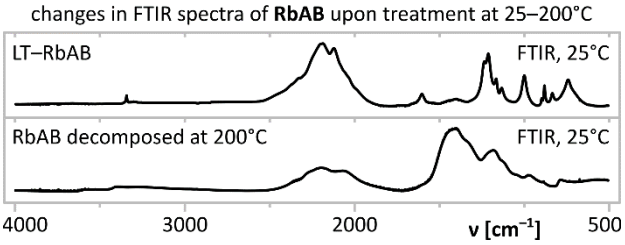

Fig. S7.1. Comparison of FTIR spectra of RbAB at various stages of thermal decomposition.

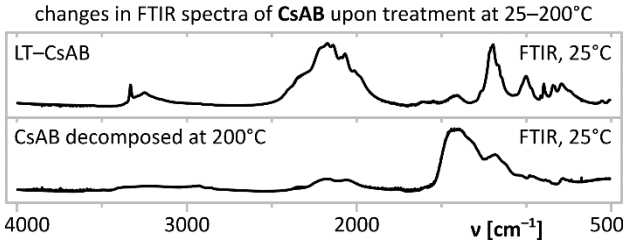

Fig. S7.2. Comparison of FTIR spectra of CsAB at various stages of thermal decomposition.

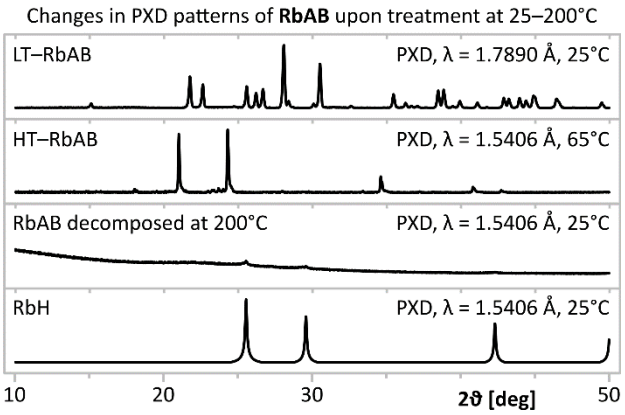

Fig. S7.3. Comparison of PXD patterns of RbAB at various stages of thermal decomposition.

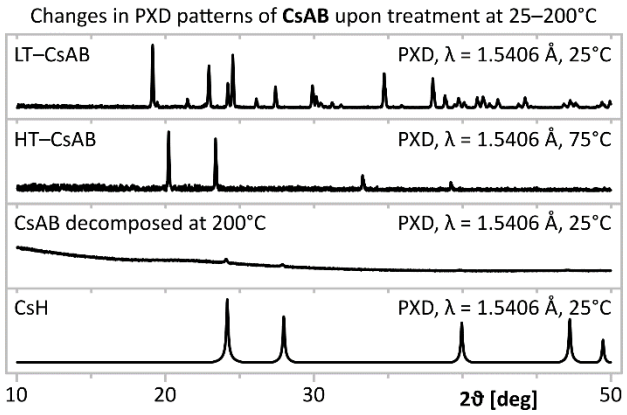

Fig. S7.4. Comparison of PXD patterns of CsAB at various stages of thermal decomposition.

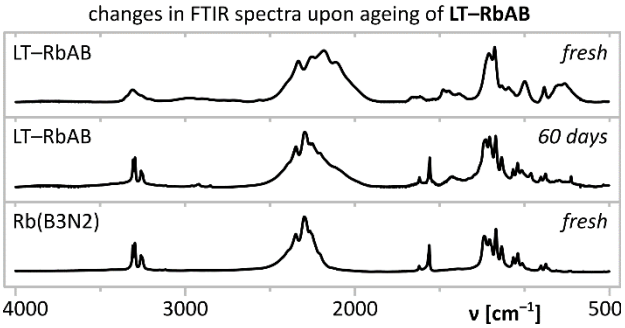

Fig. S7.5. Comparison of FTIR spectra of RbAB at various stages of ageing process with a spectrum of Rb(B3N2) salt

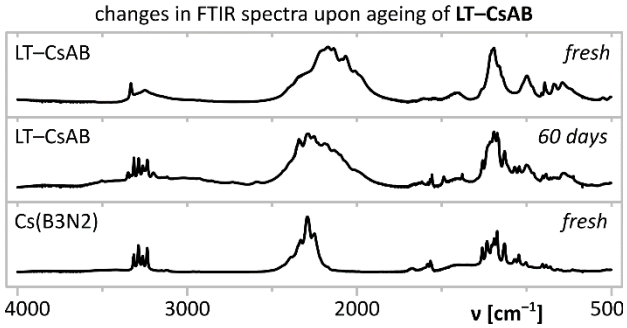

Fig. S7.6. Comparison of FTIR spectra of CsAB at various stages of ageing process with a spectrum of Cs(B3N2) salt.

8. Crystal structures and Rietveld analysis of PXD patterns [1/4]

Crystal structure of **LT–RbAB**

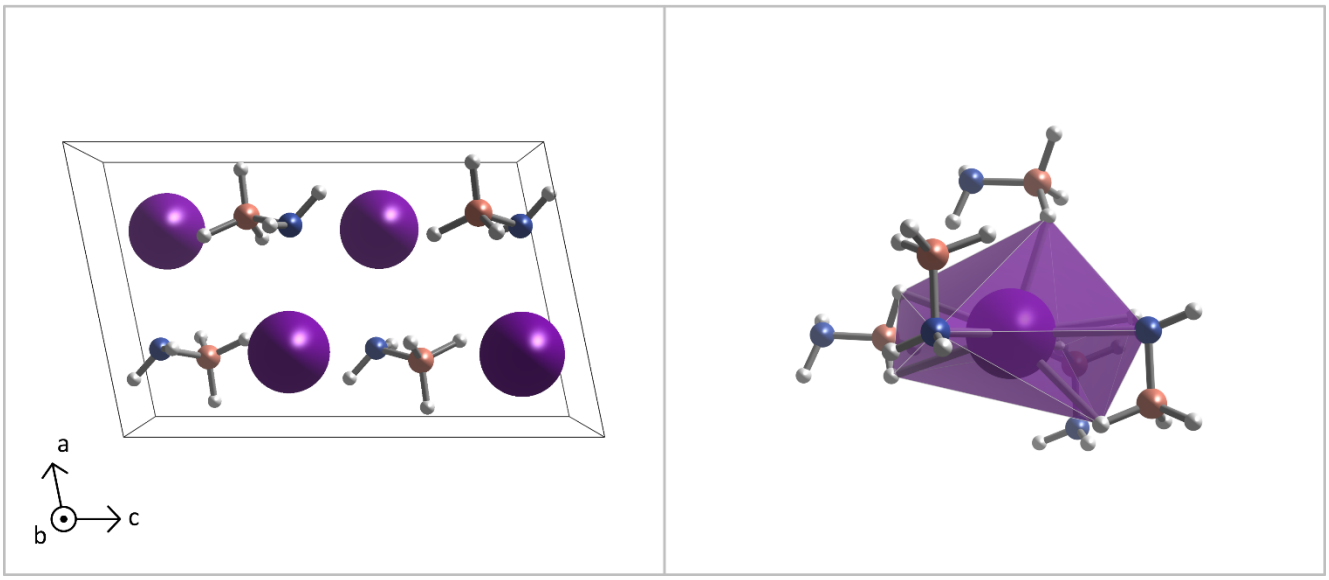

Fig. S8.1. Crystal structure of LT-RbAB.

Rietveld analysis of **LT–RbAB** PXD pattern

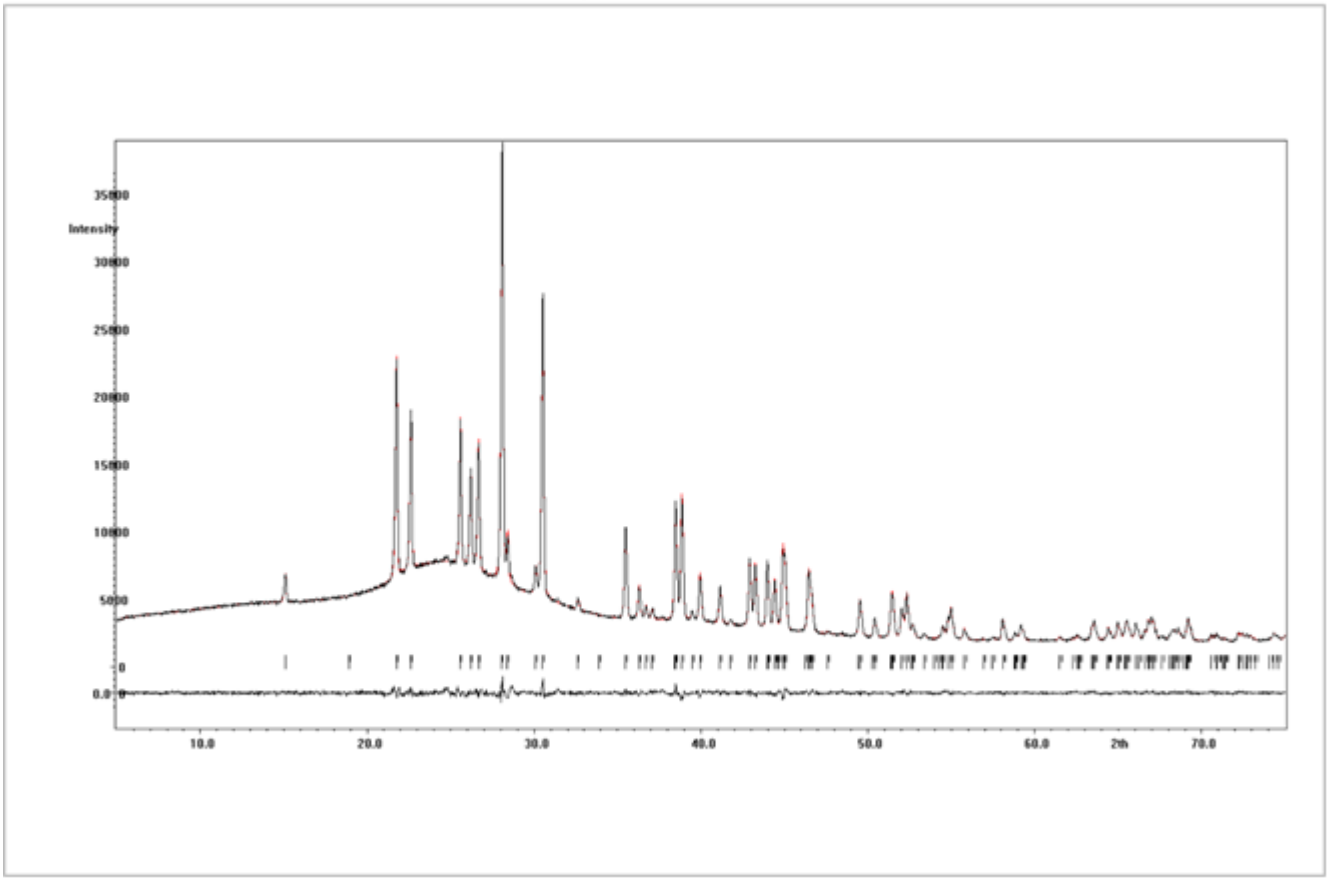

Fig. S8.2. Rietveld analysis of LT-RbAB X-ray powder pattern.

8. Crystal structures and Rietveld analysis of PXD patterns [2/4]

Crystal structure of **HT–RbAB**

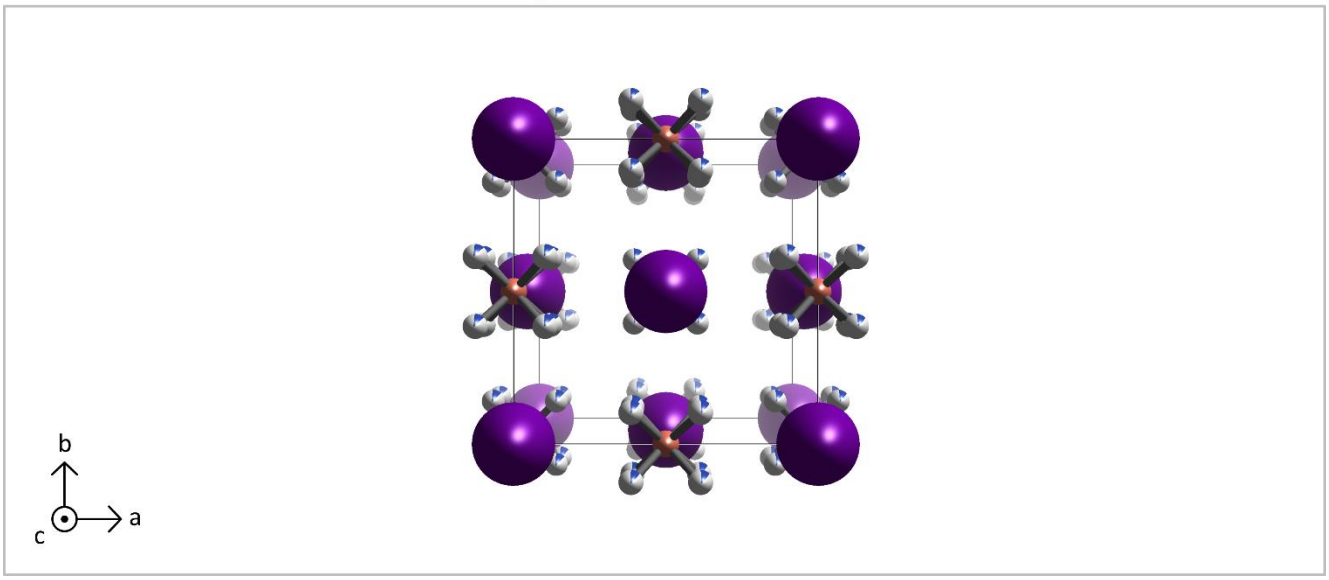

Fig. S8.3. Crystal structure of HT-RbAB.

Rietveld analysis of **HT–RbAB** PXD pattern

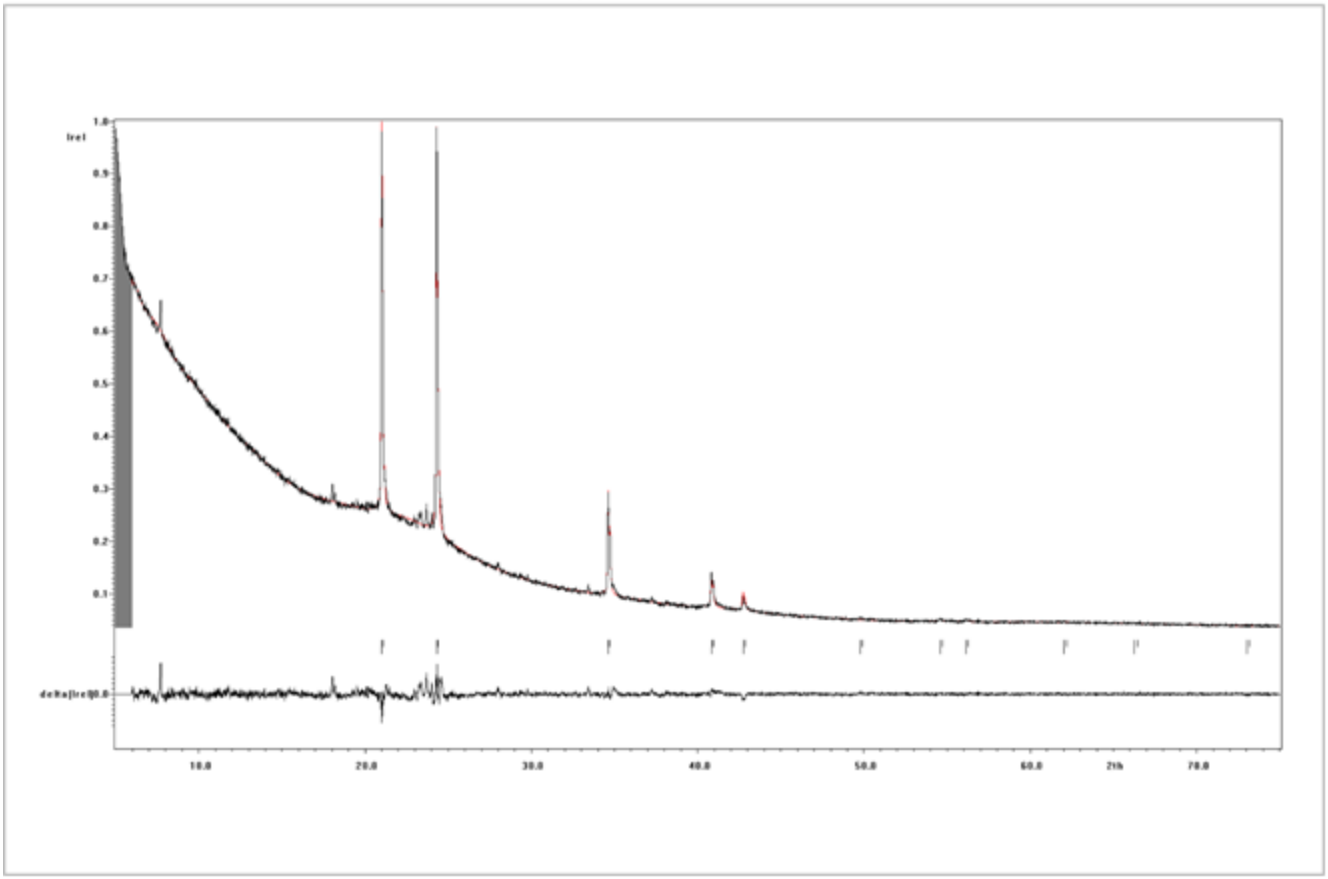

Fig. S8.4. Rietveld analysis of HT-RbAB X-ray powder pattern.

8. Crystal structures and Rietveld analysis of PXD patterns [3/4]

Crystal structure of **LT–CsAB**

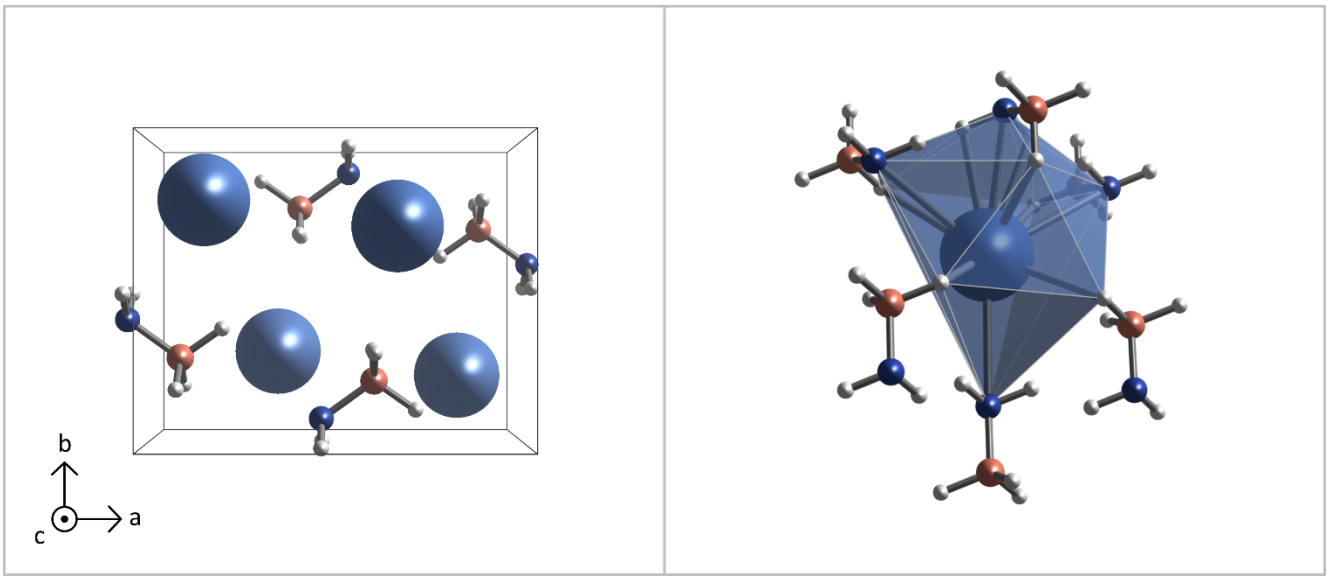

Fig. S8.5. Crystal structure of LT-CsAB.

Rietveld analysis of **LT–CsAB** PXD pattern

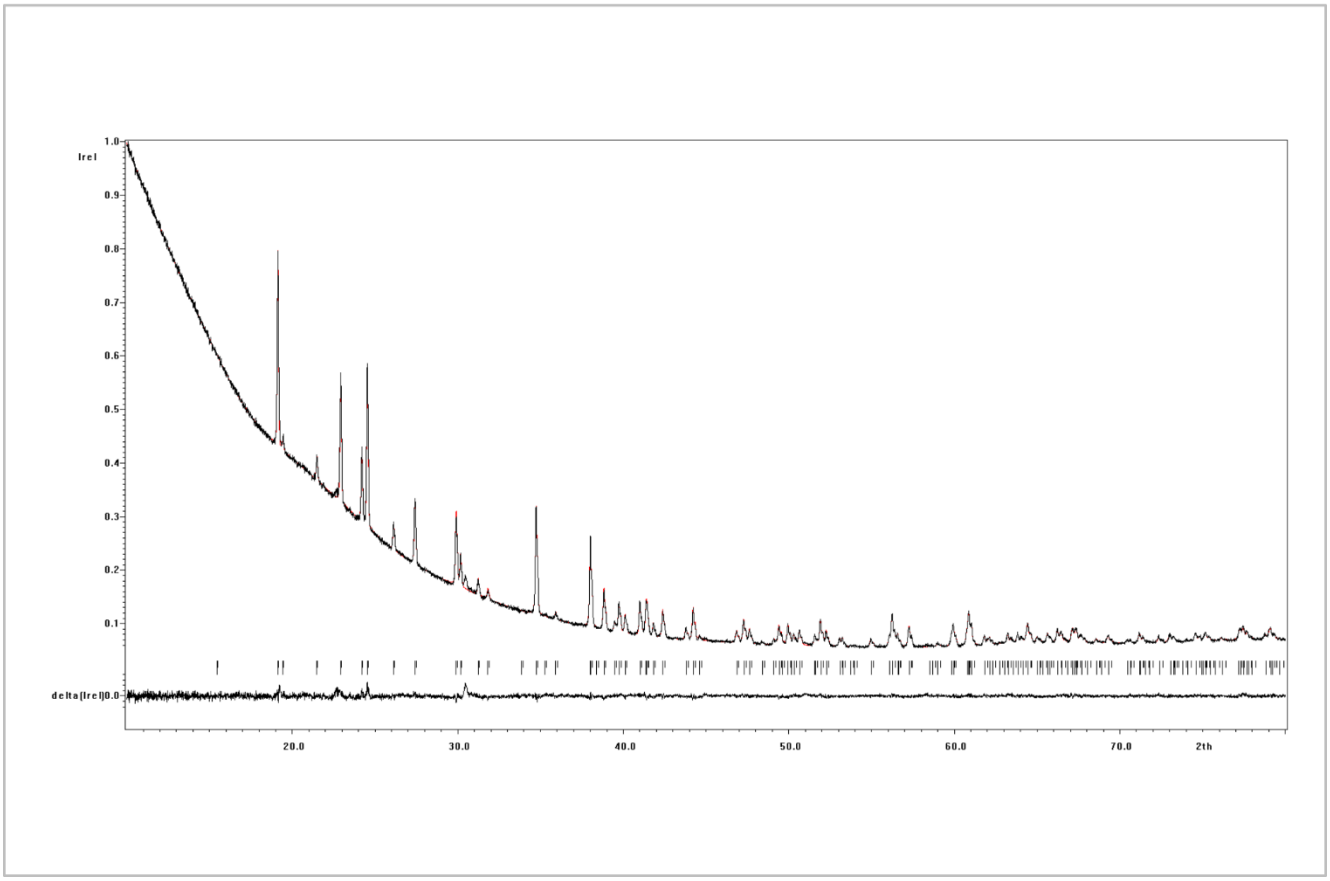

Fig. S8.6. Rietveld analysis of LT-CsAB X-ray powder pattern.

8. Crystal structures and Rietveld analysis of PXD patterns [4/4]

Crystal structure of **HT–CsAB**

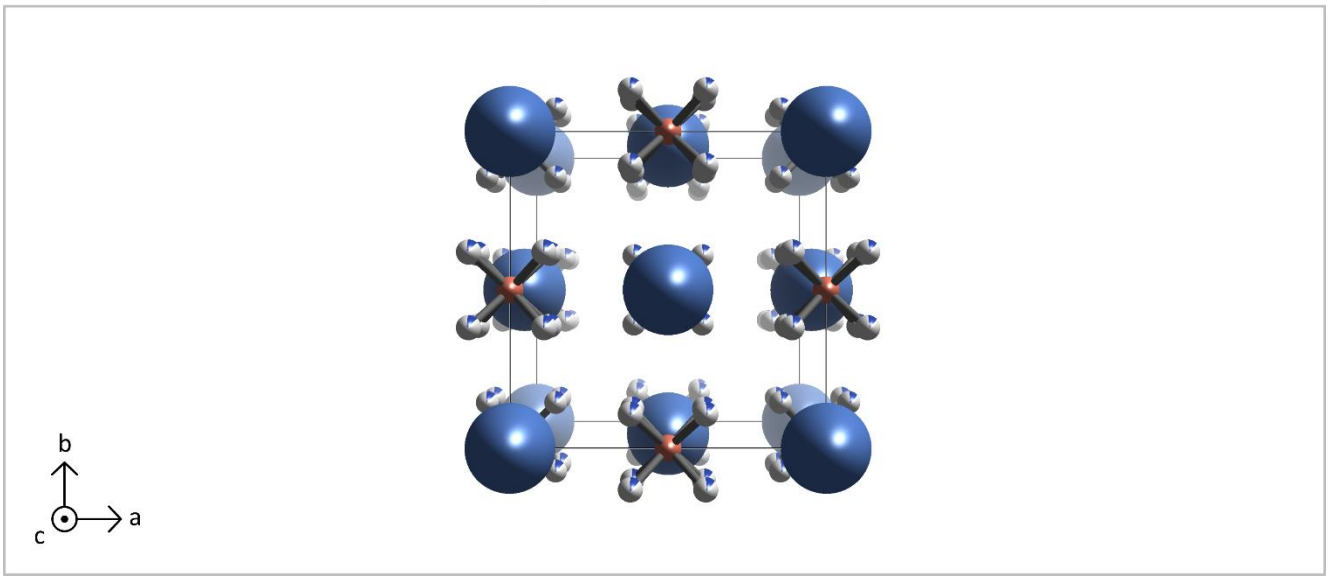

Fig. S8.7. Crystal structure of HT-CsAB.

Rietveld analysis of **HT–CsAB** PXD pattern

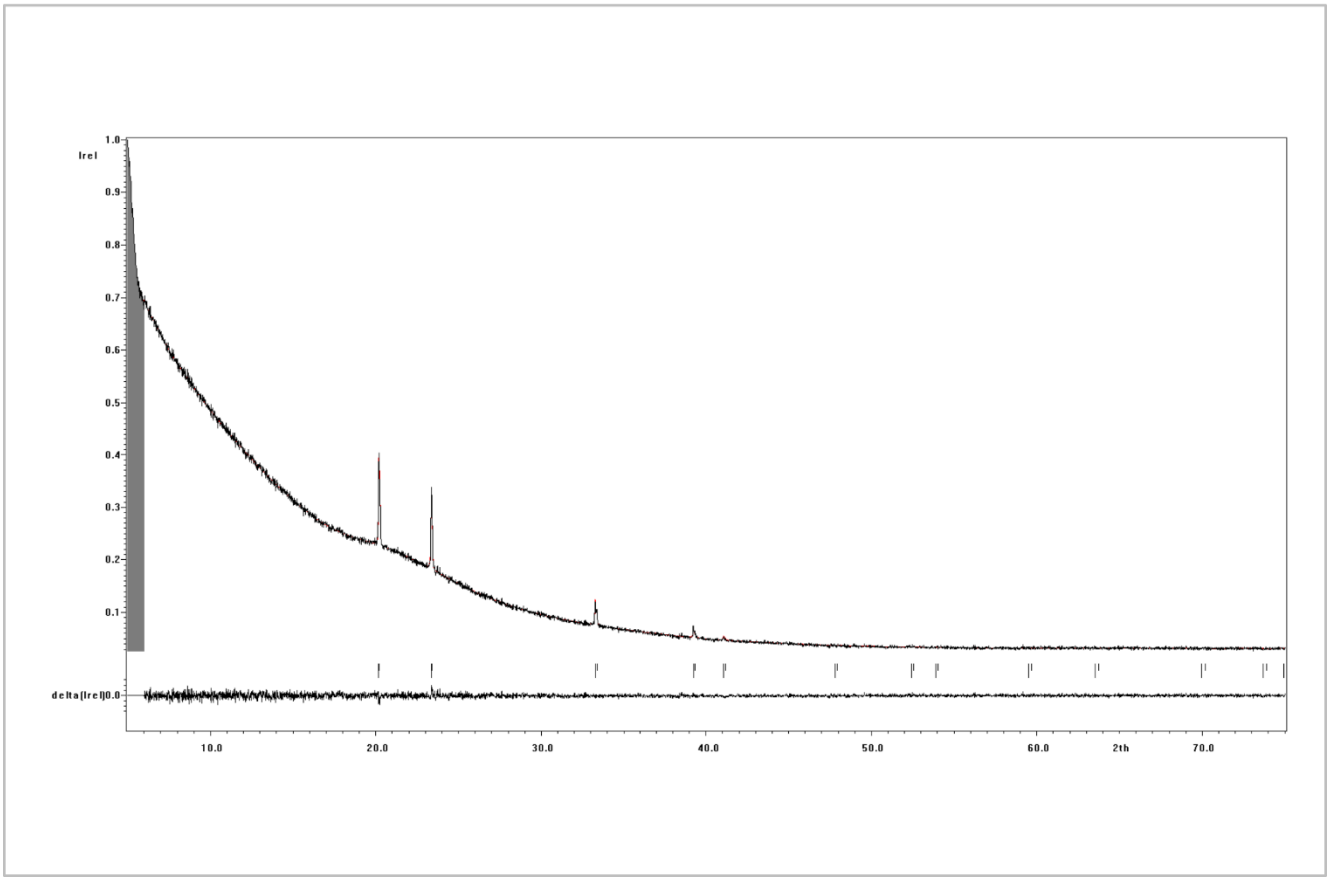

Fig. S8.8. Rietveld analysis of HT-CsAB X-ray powder pattern.

9. Comparison of FTIR, Raman, NMR, PXD data of amidoboranes and $M(BH_3NH_2BH_2NH_2BH_3)$ salts [1/2]

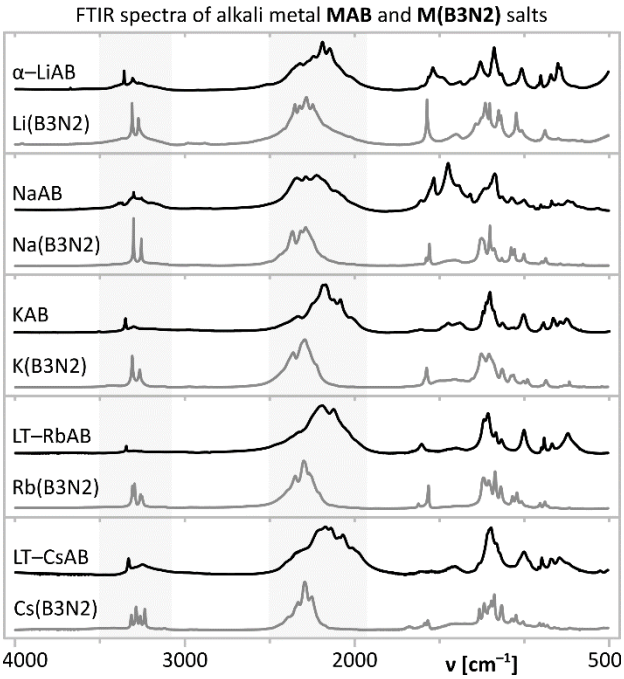

Fig. S9.1. Comparison of FTIR spectra of alkali metal amidoboranes and alkali metal M(B3N2) salts.

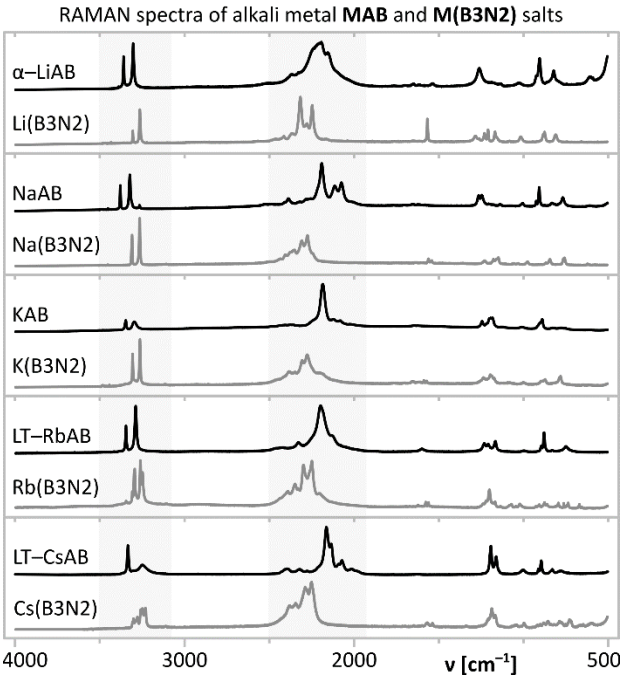

Fig. S9.2. Comparison of Raman spectra of alkali metal amidoboranes and alkali metal M(B3N2) salts.

.

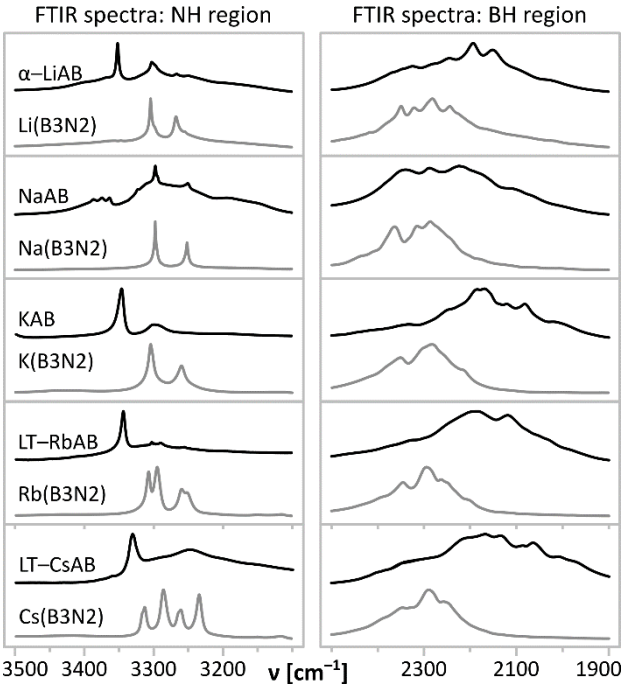

Fig. S9.3. Comparison of magnified NH stretching region and BH stretchinig region of FTIR spectra of alkali metal amidoboranes and alkali metal M(B3N2) salts.

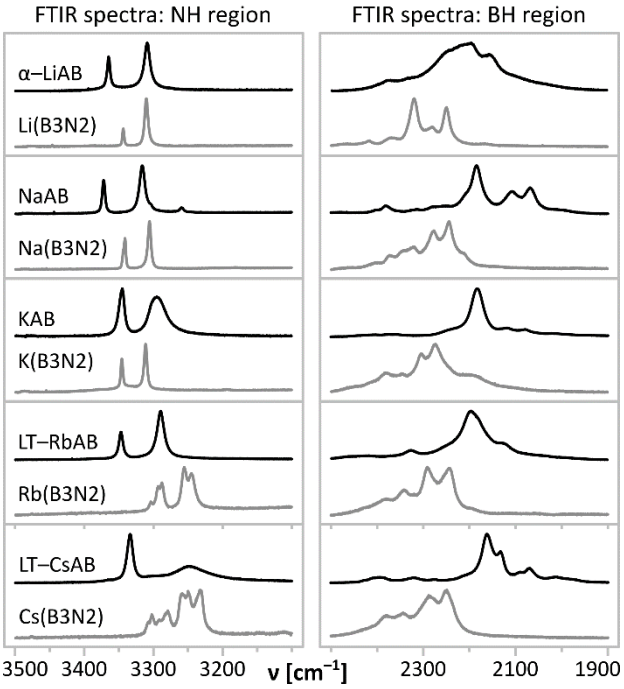

Fig. S9.4. Comparison of magnified NH stretching region and BH stretchinig region of FTIR spectra of alkali metal amidoboranes and alkali metal M(B3N2) salts.

9. Comparison of FTIR, Raman, NMR, PXD data of amidoboranes and $M(BH_3NH_2BH_2NH_2BH_3)$ salts [2/2]

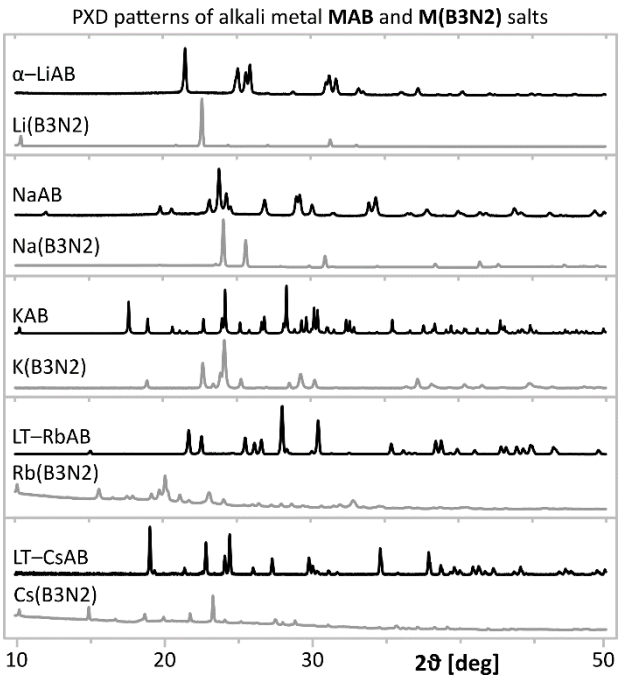

Fig. S9.5. Comparison of PXD patterns of alkali metal amidoboranes and alkali metal M(B3N2) salts.

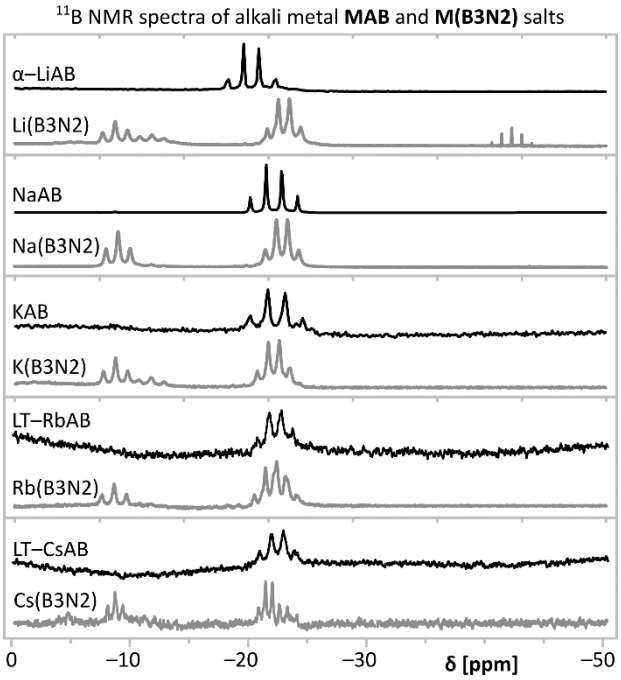

Fig. S9.6. Comparison of ^{11}B NMR spectra of alkali metal amidoboranes and alkali metal M(B3N2) salts.

10. Comparison of experimental and DFT-optimized structures of LT-RbAB and LT-CsAB [1/3]

Theoretical optimization of the crystal structure has been performed using density functional theory (DFT), as implemented in CASTEP program [S1] included in Materials Studio package (Biovia). The generalized gradient approximation (GGA) with the PBE correlation-exchange functional and ultrasoft pseudopotentials were used. The unit cell vectors were fixed at the experimental values, while the atomic coordinates were optimized using BFGS algorithm. 800 eV cut-off and a k-point grid density of *ca.* 0.05 $Å^{-1}$ were used for final optimizations and calculations of total enthalpy at 0 K. The electronic SCF convergence was $5.0 \cdot 10^{-7}$ eV per atom, while the convergence criteria for geometry optimization were as follows: energy change $5.0 \cdot 10^{-6}$ eV per atom, max. force 0.01 eV $Å^{-1}$, max. stress 0.02 GPa, max. displacement $5.0 \cdot 10^{-4}$ Å.

Table S10.1. DFT geometry optimization with experimental structures of LT–RbAB and LT–CsAB.

	LT–RbAB		**LT–CsAB**	
	experimental	**DFT**	**experimental**	**DFT**
R (M...M)	4.025(5) Å	4.069 Å	4.6007(6) Å	4.674 Å
R (M–B)	3.191(18) Å	3.216 Å	3.67(3) Å	3.254 Å
R (M–N)	3.06(1) Å	3.016 Å	3.281(13) Å	3.173 Å
R (B–N)	1.56(2) Å	1.548 Å	1.54(2) Å	1.539 Å

[S1] S. J. Clark, M. D. Segall, C. J. Pickard, P. J. Hasnip, M. J. Probert, K. Refson and M. C. Payne, *Z. Kristallogr.*, 220 (**2005**) 567.

10. Comparison of experimental and DFT-optimized structures of LT-RbAB and LT-CsAB [2/3]

Cif file of low temperature rubidium amidoborane:

LT-RbAB cif file

```
_audit_creation_method                    'Materials Studio'
_symmetry_space_group_name_H-M            'P21/C'
_symmetry_Int_Tables_number               14
_symmetry_cell_setting                    monoclinic
loop_
_symmetry_equiv_pos_as_xyz
  x,y,z
  -x,y+1/2,-z+1/2
  -x,-y,-z
  x,-y+1/2,z+1/2
_cell_length_a          6.9311
_cell_length_b          5.0150
_cell_length_c          11.0740
_cell_angle_alpha       90.0000
_cell_angle_beta        101.6880
_cell_angle_gamma       90.0000
loop_
_atom_site_label
_atom_site_type_symbol
_atom_site_fract_x
_atom_site_fract_y
_atom_site_fract_z
_atom_site_U_iso_or_equiv
_atom_site_adp_type
_atom_site_occupancy
Rb1    Rb  0.77218  0.13103  0.36750  0.10998  Uani  1.00
B1     B   0.74076  0.58823  0.16084  0.09600  Uiso  1.00
N1     N   0.77396  0.79116  0.06167  0.10400  Uiso  1.00
H1     H   0.63152  0.66259  0.23138  0.14360  Uiso  1.00
H2     H   0.66653  0.38021  0.11123  0.14360  Uiso  1.00
H3     H   0.89972  0.53055  0.22855  0.14360  Uiso  1.00
H4     H   0.82944  0.96985  0.09968  0.15590  Uiso  1.00
H5     H   0.64372  0.83944  0.00241  0.15590  Uiso  1.00
loop_
```

10. Comparison of experimental and DFT-optimized structures of LT-RbAB and LT-CsAB [3/3]

Cif file of low temperature ceasium amidoborane:

LT-CsAB cif file

```
_audit_creation_method                    'Materials Studio'
_symmetry_space_group_name_H-M            'PNAM'
_symmetry_Int_Tables_number               62
_symmetry_cell_setting                    orthorhombic
loop_
_symmetry_equiv_pos_as_xyz
  x,y,z
  -x+1/2,y+1/2,-z
  -x,-y,z+1/2
  x+1/2,-y+1/2,-z+1/2
  -x,-y,-z
  x+1/2,-y+1/2,z
  x,y,-z+1/2
  -x+1/2,y+1/2,z+1/2
_cell_length_a          9.1191
_cell_length_b          7.3445
_cell_length_c          5.9685
_cell_angle_alpha       90.0000
_cell_angle_beta        90.0000
_cell_angle_gamma       90.0000
loop_
_atom_site_label
_atom_site_type_symbol
_atom_site_fract_x
_atom_site_fract_y
_atom_site_fract_z
_atom_site_U_iso_or_equiv
_atom_site_adp_type
_atom_site_occupancy
H1      H    0.88450   0.78990   0.41732   0.05620   Uiso    1.00
H4      H    1.07707   0.52995   0.11143   0.05410   Uiso    1.00
Cs1     Cs   0.34930   0.32006   0.25000   0.02120   Uani    1.00
B1      B    0.96098   0.75910   0.25000   0.03700   Uiso    1.00
N1      N    1.01442   0.56029   0.25000   0.03600   Uiso    1.00
H2      H    1.06076   0.87652   0.25000   0.05620   Uiso    1.00
loop_
```